Title	The nature of alkanethiol self-assembled monolayer adsorption on sputtered gold substrates
Author(s)	O'Dwyer, Colm; Gay, G.; Viaris de Lesegno, B.; Weiner, J.
Publication date	2004-08-12
Original citation	O'Dwyer, C., Gay, G., Viaris de Lesegno, B. and Weiner, J (2004) 'The nature of alkanethiol self-assembled monolayer adsorption on sputtered gold substrates', Langmuir, 20(14), pp. 8172-8182. http://dx.doi.org/10.1021/la049103b
Type of publication	Article (peer-reviewed)
Link to publisher's version	http://dx.doi.org/10.1021/la049103b Access to the full text of the published version may require a subscription.
Rights	© 2004 American Chemical Society. This document is the unedited Author's version of a Submitted Work that was subsequently accepted for publication in in Langmuir, copyright © American Chemical Society after peer review. To access the final edited and published work see http://pubs.acs.org/doi/full/10.1021/la049103b
Item downloaded from	http://hdl.handle.net/10468/2886

![UCC logo]

University College Cork, Ireland
Coláiste na hOllscoile Corcaigh

The nature of alkanethiol self-assembled monolayer adsorption on sputtered gold substrates

C. O'Dwyer, G. Gay, B. Viaris de Lesegno and J. Weiner

Institut de Recherche sur les Systèmes Atomiques et Moléculaires Complexes,

Laboratoire Collisions, Agrégats et Réactivité,

UMR CNRS 5589, Université Paul Sabatier,

*118 route de Narbonne, 31062 Toulouse Cedex 4, France*

Abstract

A detailed study of the self-assembly and coverage by 1-nonanethiol of sputtered Au surfaces using molecular resolution AFM and STM is presented. The monolayer self-assembles on a smooth Au surface composed predominantly of {111} oriented grains. Domains of the alkanethiol monolayer are observed with sizes typically of $5-25$ nm and multiple molecular domains can exist within one Au grain. STM imaging shows that the (4×2) superlattice structure reverts back to a $(3 \times 2\sqrt{3})$ structure when imaged under non-contact AFM conditions. The 1-nonanethiol molecules reside in the three-fold hollow sites of the Au{111} lattice and aligned along its [112] lattice vectors. The SAM monolayer contains many non-uniformities such as pin-holes, domain boundaries and monoatomic depressions which are present in the Au surface prior to SAM adsorption. The detailed observations demonstrate limitations to the application of 1-nonanethiol as a resist in atomic nanolithography experiments for features sizes < 20 nm.

I. INTRODUCTION

Self-assembled monolayers (SAMs) of thiol-functionalized molecules on single-crystal Au surfaces have been studied by numerous groups since their discovery [1, 2]. Such organosulfur monolayers now have numerous technological applications, the most recent of which involves their use as positive resists in atomic nano-fabrication [3–8]. This application has motivated a considerable research effort focusing on their structure, assembly mechanism and experimental parameter dependencies. In the light of recent technological advances in atom beam nanolithography, a detailed understanding of the quality of coverage of the Au surface by the alkanethiol monolayer is necessary to determine its limitations as a uniform resist for feature definition on the order of $5-25$ nm.

Among the known SAMs, alkanethiols [$CH_3(CH_2)_{n-1}SH$] on Au{111} are one of the most studied systems due, mainly, to the stability and ease of preparation on atomically flat Au surfaces. From a chemical point of view, the attachment of the thiol to the Au surface is believed to proceed through a $Au-S$ bonding mechanism, which is known to be sufficiently strong and stable, with bond energies typically of ≈ 48 kcal mol^{-1} [9, 10]. Extensive X-ray photoelectron spectroscopic (XPS) experiments suggest that chemisorption of alkanethiols on gold (0) surfaces yields the gold (I) thiolate ($R-S-$) species. The presumed adsorption chemistry is,

$$R - SH + Au_n^0 \rightarrow RS^- - Au^+ + \frac{1}{2}H_2 + Au_{n-1}^0 \tag{1}$$
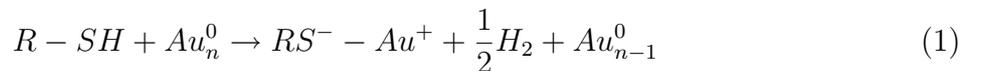
which infers an oxidative addition of the $S-H$ bond to the Au surface, followed by a reductive elimination of the hydrogen. Thus the liquid-phase formation of the monolayer is a two-step process involving chemical bonding of the molecules by diffusion to the surface followed by self-assembly aided by van der Waals interactions.

In early scanning probe microscopy studies on alkanethiols Porter *et al.* [11] observed a hexagonal lattice structure for alkyl chains [$CH_3(CH_2)_{n-1}SH$] with $n = 4-17$ using both atomic force microscopy (AFM) [12] and scanning tunneling microscopy (STM). The lattice structure is described as a $(\sqrt{3} \times \sqrt{3})R30^0$ structure, where $\sqrt{3}$ ($\equiv \sqrt{3}a$) is a multiplicative factor of the Au{111} lattice constant, a, and indicates the Au-Au interatomic distance on the Au{111} surface. $R30^0$ represents the alkyl chain, $(CH_2)_{n-1}$, tilted 30^0 away from the normal to the Au surface which is true for alkanethiols with $n = 4-17$. Using low energy electron diffraction (LEED), Dubois *et al.* [13] observed the same structure for $n < 3$ whereas for $4 < n < 12$ they reported larger unit cells $(m\sqrt{3} \times \sqrt{3})R30^0$ where m is an integer between 4 and 6 depending on the chain length). Both Porter *et al.* and Dubois *et al.* assigned the three-fold hollow site of the Au{111} lattice as the preferred adsorption site, although this had yet to be unequivocally determined.

On Au{111} surfaces, alkanethiol SAMs have an ordered structure over relatively large areas and the thickness can be controlled by using SAMs with alkyl chains of different lengths. Recently, Klein *et al.* realized a SAM on Au{111} comprising a mixture of organosulfur compounds [14]. A complex molecular arrangement on the Au{111} was observed that was attributed to the fact that chains with different lengths or head groups have different adsorption kinetics [15]. For both fundamental and applied studies of SAMs, the molecular level structure and packing arrangement is of paramount importance for the interpretation of observations, for their application in atomic nanolithography and in determining their properties. Very few studies have been conducted with SAMs on Au surfaces with orientations other than {111} and even fewer still with alkanethiols on these surfaces [16, 17]. It is widely believed that the Au{111} surface binds alkanethiols more strongly than Au{100} [18]. The structure of the alkanethiols was not examined in detail, nor was the effect of

higher grain boundary densities on the molecular package arrangement of the SAM on the surface. The long range order of alkanethiol self assembly was addressed in early STM studies [19–25] revealing that alkanethiol monolayers on Au{111}, in particular, exhibit a distribution of pit-like defects which are known not to exist on the Au surface. Although initially believed that the pits arose from missing or loosely packed alkanethiols [20–22], later studies revealed that they were in fact two-dimensional islands of Au vacancies [26] consistent with the Au{111} single-atom step height of 0.24 nm.

A.   Alkanethiol packing arrangements on Au{111} surfaces

In order to make the description of our observations clearer, this section describes schematically, the packing arrangements of alkanethiols on Au{111} surfaces. The characteristic unit mesh for each packing structure will also be defined and outlined diagrammatically. Figure 1a shows the standard hexagonal $(\sqrt{3} \times \sqrt{3})R30^0$ packing arrangement of alkanethiols on Au{111} surfaces. A cross-sectional view is shown alongside each schematic packing arrangement representing the view in the direction of the arrow. The unit mesh for such an arrangement is highlighted in the plan-view schematic in Fig. 1a. In a perfect $(\sqrt{3} \times \sqrt{3})R30^0$ hexagonal packing arrangement, all molecules are tilted 30^0 from the surface normal to the Au in the same direction and there is no variation in the height of the monolayer. Throughout this work, there are two principal variations to this structure observed when 1-nonanethiol binds to Au{111}. Both of these structures are slight variations of the hexagonal arrangement of the molecular monolayer. The first of these is the $(3a \times 2\sqrt{3}a)$ lattice, where a is the Au-Au interatomic spacing of the Au{111} lattice, equivalent to 0.29 nm. The unit mesh for this structure is illustrated in Fig. 1b. The $(3 \times 2\sqrt{3})$ lattice has been observed by means of X-ray diffraction (XRD) [27, 28], low energy atom diffraction

4

(LEAD) [29–31] and STM techniques [32, 33] for alkanethiols with $n > 8$. This unit mesh also exists in the hexagonal arrangement but the main difference is the periodic variation in the height of the molecules above the Au surface. This will be explained in more detail in section IV. The third variation is described as a $(4a \times 2a)$ superlattice, where a, again, is the Au-Au interatomic distance. This structure is outlined schematically in Fig. 1c alongside its corresponding cross-sectional view. Again, this structure is based on a hexagonal arrangement with a periodic variation (but different from that of the $(3 \times 2\sqrt{3})$ lattice) in the height of the 1-nonanethiol molecules above the surface. The superlattice is defined in the plan-view schematic.

In this paper, we present results of a detailed study of the structure of 1-nonanethiol self-assembled monolayers on a polycrystalline Au surface grown on a Cr covered Si substrate using molecular resolution scanning tunneling microscopy (STM) and atomic force microscopy (AFM). In the first section, the characterization of the Au surface prior to alkanethiol adsorption will be presented. The next section will deal with molecular resolution imaging of the monolayer and will highlight typical features of its coverage of the Au surface. The determination of the true molecular assembly of the monolayer will then be presented together with a detailed description of the non-uniformities observed in the monolayer at saturation coverage. The last two sections will present observations of monolayer non-uniformities and how these features may place limitations on realizing feature sizes of < 20 nm in nanolithography experiments. The understanding of the underlying interactions that govern the formation, packing arrangement and behavior of SAMs will provide answers to questions related to many technologically important areas. The observations presented here are motivated by the application of SAMs as resists in Cs beam atomic nanolithography [3–8, 34].

II. EXPERIMENTAL

Substrates used were Si(100) that were loaded, as-received, into the sputtering chamber. A 4 nm thick Cr adhesion layer was sputtered for 6 s at 1000 W and subsequently a 30 nm thick Au layer was sputtered for 60 s at 300 W. Both were sputtered at a base pressure of 8×10^{-6} Pa. The Au surfaces were then cleaned in ethanol and immersed in a 3:1 mixture of H_2SO_4:H_2O_2 at 398 K for 5 minutes to remove any organic contaminants. After rinsing with deionized water, the Au samples were immediately placed in a 10^{-3} mol dm^{-3} solution of 1-nonanethiol $CH_3(CH_3)_8SH$ (95%, Aldrich) in reagent grade ethanol and then incubated at room temperature for over 24 h. In the 24 h period, a self-assembled monolayer of thickness ≈ 1 nm is formed. After incubation, samples were rinsed with ethanol and examined microscopically. All atomic force microscopy (AFM) and scanning tunneling microscopy (STM) examinations were performed in ambient laboratory conditions (pressure and temperature). The crystallinity characterization was carried out by grazing incidence X-ray diffraction (GIXRD) [35] with a step width of 0.01^0, using a Philips PW-1710 diffractometer with a Cu anode (radiation K_α of $\lambda = 1.54186$ Å). X-ray rocking curves were performed on a Rigaku X-ray diffractometer with CuK_α radiation and were acquired by fixing the 2θ angle to that of the Au{111} reflection. X-ray rocking curves were acquired of the substrate and Cr layer in order to obtain the physical rocking curve of the Au overlayer by substraction and deconvolution of all spectra. AFM and STM characterization was performed with a PicoSPM (Molecular Imaging, Inc.). The STM tips were mechanically cut from 250 μm Pt/Ir (80:20) wire, electrochemically etched/polished and tested on highly ordered pyrolytic graphite (HOPG). The STM images were acquired at a bias voltage of +1.50 V in constant height mode. Images were acquired with high gap impedances to maximize the contribution

6

from the alkanethiol monolayer [33, 37], and in particular, gap impedances of $\approx 7-10$ GΩ [32] were required to resolve individual atoms. Atomic resolution STM images of monoatomic steps in a Au{111} single crystal, evaporated on mica and flame annealed was conducted in order to calibrate the vertical height. Atomically resolved STM of the Au surface used in the experiments was also conducted to determine the crystallographic orientation of the sample with respect to the STM scan direction. Atomic resolution AFM imaging was performed in both contact and AC tapping modes supplemented by lateral force and phase modulation imaging respectively. Soft Si_3N_4 tipped cantilevers with a spring constant of 0.12 nN nm^{-1} were used in contact mode. Comparisons were made with STM images to examine whether any tip-induced reconstruction of the monolayer took place during imaging under STM.

III.   RESULTS AND DISCUSSION

A.   Characterization of the gold surface

The GIXRD spectrum of the Au overlayer crystal structure is shown in Fig. 2. Two peaks were observed in the spectrum at 38.15^0 and 88.3^0, which correspond to the {111} and {222} planes of the face-centered cubic structure of bulk Au, respectively. The inter-planar spacing of the sputtered Au layer, determined from the diffraction angle of the {111} plane in Fig. 2, is measured to be 0.238 nm, in good agreement with that of the inter-planar spacing of bulk Au{111} (0.24 nm). The {111} reflection exhibits the highest relative intensity indicating that it is the preferred crystal orientation of the majority of the Au grains within the film. The physical X-ray rocking curve of the Au{111} reflection is shown in the inset to Fig. 2. Such rocking curves were acquired to determine the minimum grain size of the Au grains parallel to the film, *i.e.* the {111} oriented grains. Utilizing kinematic diffraction theory

7

[37, 38], it is known that

$$FWHM = \frac{\lambda}{2.25 d_{grain}^{\parallel}} \sin\theta \qquad (2)$$

where $FWHM$ is the full width at half maximum, $d_{grain}^{\parallel}$ is the minimum grain size parallel to the film and θ is the diffraction angle of the emerging X-rays. This approach determines the minimum grain size to be 137 ± 13 nm and the alignment of the Au grains to be {111} oriented and parallel to the surface.

The topographical AFM image of the Au surface sputtered on Cr is shown in Fig. 3a. It can be seen clearly that the surface has a grained morphology. The *rms* roughness of the sputtered Au surface, was determined from the AFM data similar to that shown in Fig. 3a, and is measured to be 1.24 nm. Such surfaces are formed by sputtering at low power, which was necessary to produce a smooth surface over a granular 4 nm thick Cr adhesion layer. This is highlighted more clearly in the magnified image of the surface in Fig. 3b.

Higher magnification AFM images of larger individual {111} oriented grains were acquired, and a typical example is shown in Fig. 4 with a height-mapped grayscale. These images were acquired in tapping mode using a Pacific Nanotechnologies Nano-R AFM. The morphology of the Au surface is consistent with 2D Stranski-Krastanov island/monolayer growth [39]. The Cr adhesion layer not only increases the adhesion of the gold to the surface but allows for 2D Stranski-Krastanov island/monolayer growth of the Au rather than the typical Volmer-Weber 3D island growth [39] of metal on semiconductors. In this image the Au surface has grown in layers where the step edges are measured to have a successive height difference of $\approx$0.25 nm, almost equivalent to the Au monoatomic step height (0.2355 nm), indicating that Au monolayers (defined in the images by the triangular terraces within the grain) are atomically flat and thus single crystal, terminated with the {111} face and delineated by the {111} crystallographic planes. Highlighted in the image are examples of

8

individual monoatomic depressions of the Au surface. Such depressions are noted to be present over the whole surface.

Thus, the sputtered Au surface is extremely smooth and is composed of grains with an average size of ≈130 nm and a preferential crystal orientation of {111} parallel to the surface. Monoatomic depressions exist on the surface of each grain prior to treatment in the alkanethiol solution.

B. Molecular resolution imaging of the monolayer

Such atomically flat surfaces, although polycrystalline, are conducive to the growth of ordered SAMs. Figure 5 shows a molecular resolution STM image of the 1-nonanethiol SAM on the sputtered Au surface. Such large scale STM surface survey images show the highly variable coverage of the Au by the SAM. The surface is observed to consist of a mosaic-like network of domains ranging in size from approximately 5−25 nm, with some defect-free domains observed to extend to more than 50 nm.

Indeed, the packing arrangement is identical and coherent within a single domain, *i.e.* all atoms are arranged such that the unit cell axes of the packing arrangement remain unchanged within the domain itself. Each of the domains are separated by domain boundaries that are typically of molecular scale dimensions. Such boundaries are identified in Fig. 5 as dark fissures between domains. Most boundaries are observed to have three orientations originating from the hexagonal Au{111} three-fold surface symmetry. However, because some of the molecular domains are smaller in dimension than the average Au grain, it must happen that termination of the SAM domains occurs through the presence of other domain boundaries or monoatomic step edges in the Au surface. It is also observed in Fig. 5 that there are two different mechanisms of boundary formation. The first is where more than one

9

SAM domain exists on a single Au grain. The boundary is formed between domains with the same packing arrangement but different alignment of their unit-cell axes with respect to each other. Figure 6a shows an example of such a domain. The second is where SAM domain boundaries are formed between domains that have the same packing arrangement and alignment (indicated within each domain by arrows in Fig. 5) with respect to each other, but exist on neighboring Au grains. A higher magnification example of such a boundary is shown in Fig. 6b. These Au grains must have the same terminating crystal face but are oriented differently with respect to each other.

We believe the boundary formation between neighboring Au grains is due to the presence of Au step edges, because it is difficult to obtain dense packing of alkanethiols at Au step edges. Alkanethiols are believed to bond at the three-fold hollow sites between the hexagonal arrangement of Au atoms on a Au{111} surface [11, 12, 29–32]. Consequently, at a step edge, Au atoms on the upper terrace exist as an adlattice in the three-fold hollow sites of the lower Au terrace. This occupancy causes a mismatch in the positioning of the SAM molecules, which would ordinarily have occupied these positions, resulting in a lower density of SAM molecules in the vicinity of the boundary.

STM imaging also highlights the presence of features on the surface that appear as pronounced dark circular topographical depressions which apparently contain no SAM. These depressions are highlighted in Figs. 5 and 6b. Line scan analysis of these images reveals that these depressions are approximately 0.25 nm in depth, which is very close to the Au{111} terrace step height, indicating that these are monoatomic pits in the Au surface. These pits were also observed by other groups with alkanethiols of different chain lengths [19, 32], and it had been previously concluded that the depressions were etch pits, formed by a corrosion process during thiol adsorption. Results presented here for sputtered Au on Cr show

remarkable similarity to the 'etch pits' observed in Refs. [19, 32] and puts into question this interpretation. It is clear from Fig. 4 that monoatomic pit-like depressions exist in the Au surface *prior* to thiol self-assembly and their density is commensurate with the higher magnification STM images of the SAM-on-Au. The fact that no molecular resolution of thiol molecules within these depressions is observed is primarily due to the fact that, under constant height STM conditions, the extra distance of ≈0.25 nm renders the tip-surface distance too great for detection of the electronic surface state of either the outermost methyl chain or the Au−S bond and thus no tunneling current is detected. The STM images will be compared to high resolution AFM images of the alkanethiol monolayer in section IV.

Thus, alkanethiol monolayers on Au{111} crystal faces exhibit many non-uniformities at saturation coverage. Domain boundaries and monoatomic depressions in the monolayer were observed with STM. The monoatomic depressions are those present on the Au surface prior to SAM adsorption and we believe that the SAM covers both the surface and the pit-like depressions.

IV. HIGH-RESOLUTION IMAGING: DETERMINATION OF MOLECULAR ASSEMBLY

In Fig. 7, high resolution STM and AFM images of the molecular packing arrangement of the SAM on Au are shown. Figure 7a is a constant height STM image and Fig. 7b is a non-contact AFM image of the same surface. Both techniques were employed to deduce the effect of tip-surface interactions in the determination of the true self-assembly process of alkanethiols on Au.

A zig-zag pattern (denoted by open circles in Fig. 7a) is evident within this packing arrangement that is a slight variation of the $(\sqrt{3} \times \sqrt{3})R30^0$ packing arrangement discussed

in detail by previous authors [19, 27, 32]. The primitive unit mesh is highlighted for clarity and is measured to have lattice dimensions of 1.2 nm × 0.55 nm. These dimensions are consistent with the lattice constants $\alpha = 1.15$ nm and $\beta = 0.58$ nm of a $(4a \times 2a)$ super-lattice [33], where a is the interatomic spacing of the Au{111} lattice and $\alpha = 4a$ and $\beta = 2a$. However, many groups [1, 32, 35] have reported that STM induces irreversible changes in the molecular arrangement, especially when constant height imaging is performed with high magnification. Poirier [32] observed that the arrangement of octanethiol SAMs was transformed from the $(3 \times 2\sqrt{3})$ unit mesh to the $(\sqrt{3} \times \sqrt{3})R30^0$ arrangement, and attributed this transformation to electronic effects that could be avoided by adjustment of the magnitude or sign of the bias voltage. However, regardless of the adjustments made, STM imaging, even with relatively high tunnel gap impedances, *can* affect the molecular arrangement. This effect is observed because the tip is essentially scanning in the monolayer itself. The (4×2) superlattice in the STM image in Fig. 7a is seen as a skewed $(\sqrt{3} \times \sqrt{3})R30^0$ hexagonal arrangement. In using the molecular resolution non-contact AFM image in Fig. 7b, we have been able to determine the true arrangement of 1-nonanethiol on Au{111}. Figure 7b shows such an image and the basic hexagonal $(\sqrt{3} \times \sqrt{3})R30^0$ arrangement is observed. From this image, neighboring molecules are observed to be separated by a distance equal to $\sqrt{3}a \approx 0.5$ nm, where a is the interatomic distance on a Au{111} surface (0.29 nm). In other words, the separation between 1-nonanethiol molecules is similar to the distance between second-neighboring [110] Au rows. This implies that molecules are bound either in equivalent three-fold hollow sites on the Au{111} surface or directly on top sites of Au{111} for which the same lattice vectors are expected. Consequently, the 1-nonanethiol monolayer is commensurate with the Au adlattice along its [112] directions. Such commensurability probably allows for good long range order within each domain, an example of which can be

12

seen in Fig. 5.

In the (4 × 2) structure in Fig. 7a, in contrast to the $(\sqrt{3} \times \sqrt{3})R30^0$ structure, half of the alkyl chains must either be twisted clockwise or anticlockwise around their main molecular axis, resulting in different orientation of the topmost C−C bond. To form a (4 × 2) structure, it must happen that every second C−C bond at the surface be twisted clockwise or anticlockwise, by approximately $\pm50^0$ around their main axis. Such rotations form the zig-zag pattern observed in a single line of 1-nonanethiol molecules along the [112] direction of the Au{111} surface. To account for the differences in C−C bond position, we consider that the molecular positioning observed in Fig. 7a is described in terms of discrete twists of the all-trans hydrocarbon backbone of the 1-nonanethiol molecule while maintaining the original tilt angle of 30^0 to the surface normal. The schematic of the different arrangements is shown in Fig. 1.

At this point it is instructive to outline the detail of conformational isomers which describe the structure of the alkanethiol molecular chain. In acyclical structures, such as 1-nonanethiol, rotation about a single bond can produce an infinite number of arrangements. These can be divided into three catagories: *cis*, *trans*, and *gauche*. The plan-view diagrammatic representation of each of these three conformations for two CH_2 groups of the alkyl chain found in an alkanethiol molecule, $(CH_2)_{n-1}$ are shown in Fig. 8a. The *trans* conformation means that each successive carbon atom is at 180^0 to the previous one, whereas the *cis* conformation displays eclipsing of the carbon atoms as each successive carbon atom is equi-aligned. 1- nonanethiol molecules are in an all-trans conformation, which results in the zig-zag shaped chain protruding from the surface. This can be seen schematically in Fig. 8b. The gauche conformation results from the angle between two successive carbon atoms in the chain being less than 180^0 while still maintaining its tetrahedral structure with the

13

hydrogen atoms. However, *cis* conformations are never observed in these molecules. Thus, a pair of successive gauche conformations within the 1-nonanethiol molecular chain can result in rotational motion of the chain at the position where the defect is located. This rotation reduces the instability induced when two successive gauche conformations are aligned with each other. It has been shown that the formation of gauche defects in the S−C bonds near the Au surface, that can result in kink defects in the alkyl chains, accompany alkanethiol rotational motion [40]. However, it has been shown that alkanethiols at room temperature display almost no axial rotations [40]. Under conditions where rotation *is* possible, several groups have shown that multiple discrete rotations are observable [41]. Conditions where rotations are possible include elevated temperatures and application of mechanical force. A recent molecular dynamics study using an all-atoms model has shown that these possibilities are limited to four rotation angles for alkanethiols on Au [42].

Thus, having clarified the conformations possible within an alkanethiol molecular chain, the analysis of the observations in Fig. 7a and 7b was accomplished using the following considerations. The H−C−H bond angles were set equal to the ideal tetrahedral angle. Also, the Au−S−CH$_2$ angle was not subject to any bending. The whole chain was set to be in an all-trans configuration tilted 30^0 from the normal to the Au surface. It is assumed that a single gauche defect is unlikely to exist in the middle of a chain because in a densely packed monolayer system, the bend formed by a gauche bond in the center of the chain would be prohibited energetically. One way to accommodate a gauche defect is to form a kink, *i.e.* a pair of successive gauche conformations in the chain. Thus, a clockwise rotated gauche conformation and a counterclockwise rotation gauche conformation separated by a *trans* bond can accommodate the kink and still maintain the linearity of the molecular chain. Thus, if rotation of the molecular axis is permitted at the point of a gauche defect, then the

14

molecules act as apparent hindered rotators, as described by Mar *et al.* [40]. We believe that this rotation effect causes the variation in the height of the terminal methyl group above the surface of the Au.

Analysis of Figs. 7a and 7b shows that an alternate rotation of $\approx 50^0$ is necessary to change from the $(\sqrt{3} \times \sqrt{3})R30^0$ packing to the (4×2) structure with a corresponding precession about the surface normal of $\approx 12^0$ away from the nearest neighbor position. This observation is in good agreement with other experimental observations on different organic monolayers and with the molecular dynamics study of Mar and Klein [40]. The twists also result in different height levels for the terminal methyl group. Repositioning of molecules on the surface is possible due to STM tip interactions [32, 43], especially if such interactions result in the rotation of the molecule around its principal axis. It is reported [43] that an STM tip or a friction force microscopy tip induces structural changes of dodecanethiol SAMs on Au{111} due to the large repulsive force (> 30 nN) of the tip pressing upon the surface. Thus, even attractive force interaction may change the molecular arrangement although we cannot conclude what the detailed mechanisms are as yet. Thus, the surface at room temperature is essentially in a crystalline state where all chains are tilted 30^0 away from the surface normal to the Au. Previous studies have shown that the alkyl chains are essentially free of gauche defects below 300 K, and so few tilt defects are expected during self-assembly at room temperature. Furthermore, the differences observed in Fig. 7 are considered to be linked to the method of observation, namely, the proximity of the STM tip under bias to a soft organic monolayer with a highly periodic structure. This physical rotation of $\pm 50^0$ is due to the monolayers susceptibility to spatially limited molecular rotation around its alkyl chain axis.

High resolution AFM and STM imaging has enabled us to identify the true structure

of 1-nonanethiol on Au{111} surfaces formed by sputtering. AFM imaging highlights the effect of tip-surface proximity by showing that the (4×2) superlattice reverts back to the $(3 \times 2\sqrt{3})$ unit mesh of a hexagonal packing commensurate with the Au{111} lattice. Furthermore, the unit mesh contains four SAM molecules. The tip-induced difference can be quantified by periodic differences in the height of the methyl headgroup of every second SAM molecule. This height variation is caused by rotation of the molecule about the alkyl backbone by $\pm 50^0$. The monolayer is observed to be commensurate with the Au lattice along its [112] directions.

V. STRUCTURE AND DOMAIN FORMATION OF 1-NONANETHIOL ON AU{111}

A. The true structure of 1-nonanethiol on Au{111}

The molecular resolution non-contact AFM image in Fig. 7b shows a rectangular primitive unit mesh of the characteristic $(3 \times 2\sqrt{3})$. The measured cell dimensions are 0.99 nm $\times$ 0.86 nm and are very close to the theoretically expected values of 1.01 nm $\times$ 0.85 nm. It is four times greater than that of the unit cell of a $(\sqrt{3} \times \sqrt{3})R30^0$ arrangement. This unit mesh outlined in the AFM image is observed to contain four molecules, which is in agreement with STM images, helium and X-ray diffraction of shorter chain alkanethiol layers on Au [16]. It has been reported that this mesh can be described as a (4×2) superlattice in terms of the $(\sqrt{3} \times \sqrt{3})R30^0$ hexagonal packing arrangement [32]. However, examination of the brightness of each molecule comprising the unit cell shows the regular periodicity in the form of the $(3 \times 2\sqrt{3})$ unit mesh, as outlined in the molecular resolution topographical AFM image in Fig. 9. This observation suggests that all molecules, if bound in equivalent

Au lattice sites, portray some variation in their extension from the bonding point. This variation could arise from a molecular orientation of the alkyl chain in a manner similar to that described for the (4×2) structure in Fig. 7a, or structural kinks due to gauche kink defects within the all-trans hydrocarbon backbone. Because this information was acquired using AFM (a topographical technique), the effect cannot be ascribed to variation in the Au$-$S bonding hybridization or artifacts of STM imaging due to tip-surface height variations over a non-conducting organic layer. Furthermore, these observations cannot be ascribed to the intermittent detection of electronic states from either the Au$-$S bond, S$-$C bond or the hydrocarbon chain. The corresponding repeat distances of the molecular ordering are quantified in the cross-sectional profiles in Fig. 9.

The unit mesh highlighted in Fig. 9 is that of the $(3 \times 2\sqrt{3})$ within a hexagonal $(\sqrt{3} \times \sqrt{3})$R30^0 molecular packing arrangement. This unit mesh is quantified in the adjoining line scan profiles where the repeat distances of neighboring molecules $(\sqrt{3}a)$ and next-nearest neighbor molecules $(3a)$, derived from topographical AFM images of the surface, are shown. Thus, the true self-assembled arrangement of 1-nonanethiol on Au$\{111\}$ is a hexagonal arrangement commensurate with the Au$\{111\}$ lattice along its [112] directions with a unit mesh defined by $(3a \times 2\sqrt{3}a)$ containing four SAM molecules.

B. Domain boundary formation in alkanethiol monolayers

The different possible registries of the hexagonal $(\sqrt{3} \times \sqrt{3})$R30^0 as either a $(3 \times 2\sqrt{3})$ unit mesh or a (4×2) superlattice can result in the SAM monolayer adopting a number of symmetry-equivalent packing arrangements commensurate with the Au$\{111\}$ lattice to which it is bound. Over a 24 h incubation period in ethanolic based alkanethiol solution, certain growth conditions can occur where the distance between nucleation events is less than

the terrace size and various domains can nucleate, grow and coalesce with the formation of a network of domain boundaries. Poirier *et al.* [32] in a study of octanethiol monolayers on Au{111} surfaces, report SAM coverage with a much greater density of depressions in the surface topography and further postulate that the SAM domain size is controlled by this density. Our observations show that the density of monoatomic depressions in a SAM layer is not the sole condition that determines the domain size. The presence of depressions in the Au surface and evidence shown for multiple domains on a single Au grain suggest that a crucial factor in the realization of defect free alkanethiol monolayers is the quality of the Au surface. Details on the dependency of SAM coverage on the quality of the Au surface will be presented elsewhere [34].

Figure 10a shows a detail of a domain boundary on the (4 × 2) superlattice observed by STM. The position of the boundary along two main axes of symmetry is indicated in the image. This translational boundary results in the displacement or translation of the (4 × 2) superlattice SAM by one nearest neighbor distance of the Au{111} lattice. In Fig. 10b a region of high density step edges can be observed, with each step covered with SAM molecules. The steps are Au{111} step edges and are all delineated by the {111} planes of the Au lattice. The Au steps vary in width from approximately 0.5−2 nm. A third class of boundary observed in the monolayer assembly are rotational boundaries. These types of boundaries are formed when the unit mesh packing arrangement rotates around an axis, defined by a directional lattice vector of the Au lattice. The rotational boundaries do not display physical molecular-scale fissures like other boundaries such as antiphase, translational and twin boundaries or stacking faults. Figure 10c shows the presence of rotational boundaries within the monolayer. The rotational boundary is indicated by the dashed line. Thus the boundary is ordered with molecular features occupying all dense-

18

packed lattice sites of the Au surface. The unit mesh is maintained but the superlattice is rotated about the {112} plane of the Au lattice. The direction of the rotational boundaries are always along the unit cell axis of the superlattice. Since the size and density of SAM domains are defined by the amount of boundaries, the presence of continuous rotational boundaries implies that the density of monoatomic depressions in the alkanethiol monolayer cannot be the only limiting factor that determines domain size. A prominent Au step edge can also be seen in Fig. 10c. The lower density molecular coverage immediately prior to the step can also be observed and occurs due to the reasons outlined in section III(B). This monoatomic step shows the hexagonal molecular overlayer packing arrangement and how this arrangement leads to a non-planar terrace boundary. The alignment of the SAMs is such that the unit cell short axis is parallel to the [111] directions of the Au lattice and the long axis is parallel to the [112] directions. The observation of the 'sawtooth' molecular arrangement at the step edge gives the first direct microscopic confirmation that the 1-nonanethiol molecules are bound to the three-fold hollow sites of the Au lattice and not on the bridge sites between Au atoms. This observation can be also seen quite clearly by referring to the schematic arrangement in Fig. 1 and noting the sawtooth pattern of the molecular arrangement at the left edge of the schematic Au lattice. Such boundaries are indicative of significant non-uniformity on the nanometer scale, implying limitations on the resolution of patterning achievable when SAMs are employed as positive resists in atomic nanolithography experiments.

These observations were all made on Au{111} single crystal grains. Even with exceptionally ordered sputtered Au surfaces composed of predominantly {111} terminated Au planes, the relative orientation of each Au{111} grain with respect to another would also add to the density of features that make the molecular coverage non-uniform. This crystal-grain

non-uniformity will be addressed in more detail in the next section.

In summary, molecular resolution AFM confirms the hexagonal overlayer structure with a $(3 \times 2\sqrt{3})$ unit mesh. The SAM layer is observed to contain both translational and rotational boundaries. The presence of numerous step edges had also been observed. The Au surface quality and the terrace size influence the density and size of SAM domains. If nucleation of SAM binding events on a single Au grain is smaller than the terrace size, they can occur independently, resulting in separate domain formation and increased non-uniformity. This separate SAM domain formation on a single Au grain shows the limit to the minimum feature size that can be realized in atomic nanolithography experiments is ≈ 20 nm.

C.   Surface uniformity of 1-nonanethiol monolayers on Au{111}

The detailed study of the self-assembly of 1-nonanethiol of Au{111} described in the previous sections has given valuable information on the eventual quality of the monolayer at saturation coverage. The uniformity in the coverage is limited by monoatomic depressions in the Au surface, the formation of domain boundaries with the SAM layer itself (even within the domain boundaries of a single Au grain) and variation in the density of SAM packing on the surface. Another observation was the inadequacy of STM imaging techniques to truly identify the actual structure of the monolayer while simultaneously giving quantitative information on the quality of the coverage. Under conditions where tip-induced artifacts are minimized, resolution of SAM coverage on Au surfaces of variable height, *i.e.* on various Au terraces, is difficult. Thus, as mentioned in section IV, we employed AFM topographical techniques together with supplementary STM imaging to study the interface between mono-layer domains. This technique was used to determine the packing density between domains

where the respective structure and packing arrangement are identical. Such boundaries are most often observed between SAM domains large enough to be considered functional for potential nanometer scale pattern definition in atomic nanolithography.

Fig. 11 shows an STM image of the 1-nonanethiol on Au, where a large number of non-uniformities and defects are observed. Such images have allowed us to address questions on SAM coverage that are still in debate. For instance, on areas of the surface where many small $(3-5$ nm) SAM domains are observed, multiple boundary types co-exist in close proximity, thus rendering a much greater percentage of the functional surface useless for nano-scale pattern definition. A striking observation is the presence of a prominent hole in the SAM layer with an effective maximum diameter of almost 25 nm. The depth of this depression is of the order of a few monolayers of Au, $i.e.$ it is not solely a monoatomic depression in the Au lattice. These relatively deep vacancies have a much lower surface density than the monoatomic depressions of the Au surface, but we do not know the details of their origin as of yet. It has been postulated that such vacancies could have occurred through dissolution of the Au during the SAM growth process [19, 26, 39].

Previous STM studies of the surface of alkanethiol covered Au{111} claimed that, within a single domain, no irregularities are found. However, by conducting a large scale survey of 1-nonanethiol coverage on Au, the first observation of the presence of pinhole defects within the domain was observed and can be seen in Fig. 11. These molecular-scale pinholes are predominantly observed in areas where the non-uniformity is most excessive. Examples of pinholes with diameters of $0.5-1$ nm can be seen in the lower left part of Fig. 11.

Fig. 12 shows a molecular resolution non-contact AFM image of the boundary between two SAM domains. The boundary is observed to run directly down the center-left of the image. It can be seen, that, although the density of the molecular coverage is less in the

21

vicinity of the boundary, the center of the boundary has coverage densities commensurate with that of the surface. This implies that SAM domain boundaries that have a width on the nanometer scale can accommodate SAM molecules only if the SAM domains are formed on a surface with the same crystal orientation and alignment. On such surfaces, *i.e.* on a single Au grain, no translational boundaries are formed. Furthermore, the AFM data does not readily show the presence of monoatomic depressions. This observation can be ascribed to that fact that thiol coverage remains unchanged for height variations on the order of one Au adlattice, a conclusion that is not apparent from just STM studies of the surface. Thus, using both AFM and STM studies, we have been able to verify that the surface within 1-atom deep depressions are covered with SAM molecules.

VI. CONCLUSIONS

This work has delineated the true structure of 1-nonanethiol self-assembled monolayers on sputtered Au surfaces by using molecular resolution STM and AFM imaging. The monolayer self-assembles on an extremely smooth Au surface that is composed of predominantly {111} oriented grains with a typical size of $25-40$ nm. Long-range order domains of the alkanethiol monolayer are observed with sizes typically of $5-25$ nm and multiple molecular domains can exist within one Au grain. The STM images show that the (4×2) superlattice structure reverts back to the $(3 \times 2\sqrt{3})$ structure when imaged under non-contact AFM conditions. There are a range of possible mechanisms for this structural change. Firstly, the change in the force interaction between the tip and the surface depending on the tip-surface distance induces the apparent structural change. Second, the change in the twist of the alkyl chains induced by the attractive force interaction varies the surface topography. The SAM also displays many discontinuities in its coverage of the Au surface, varied domain boundaries

and depressions, that arise from monoatomic variations in the Au lattice underneath. It has also been established that these depressions exist on the Au surface prior to and during the adsorption of alkanethiols. These high resolution studies have not only clarified the true structure of 1-nonanethiol on Au{111} but have resolved the debate on whether domain boundaries are bounded by monoatomic depressions. We have showed that this is not the case. The first direct evidence that the 1-nonanethiol molecules must reside in the three-fold hollow sites of the Au lattice has also been presented. The observation of a high density of domain boundaries, pin-holes and monoatomic depressions may limit the applicability of these self-assembled monolayers on Au surfaces at nanometer feature sizes < 20 nm.

References

[1] Schreiber, F. *Prog. Surf. Sci.* **2000**, *65*, 151

[2] Ulman, A. *Chem. Rev.* **1996**, *96*, 1533

[3] Meschede, D.; Metcalf, H. *J. Phys. D.: Appl. Phys.* **2003**, *36*, R17 and references therein

[4] Camposeo, A.; Cervelli, F.; Piombini, A.; Tantussi, F.; Fuso, F.; Allegrini, M.; Arimondo, E. *Mat. Sci. Eng. C* **2003**, *23*, 217

[5] Kreis, M.; Lison, F.; Haubrich, D.; Meschede, D.; Nowak, S.; Pfau, T.; Mlynek, J. *Appl. Phys. B.* **1996**, *63*, 649

[6] McClelland, J. J.; Scholten, R. E.; Palm, E. C.; Celotta, R. J. *Science* **1993**, *262*, 887

[7] Berggren, K. K.; Bard, A.; Wilbur, J. L.; Gillaspy, J. D.; Helg, A. G.; McClelland, J. J.; Rolston, S. L.; Phillips, W. D.; Prentiss, M.; Whitesides, G. M. *Science* **1995**, *269*, 1255

[8] Nowak, S.; Pfau, T.; Mlynek, J. *Appl. Phys. B* **1996**, *63*, 203

[9] Dubois, L. H.; Nuzzo, R. G. *Ann. Phys. Chem.* **1992**, *43*, 437

[10] Schlenoff, J. B.; Li, M.; Ly, H. *J. Am. Chem. Soc.* **1995**, *117*, 12528

[11] Widrig, C. A.; Alves, C. A.; Porter, M. D. *J. Am. Chem. Soc.* **1991**, *113*, 2805

[12] Alves, C. A.; Smith, E. L.; Porter, M. D. *J. Am. Chem. Soc.* **1992**, *114*, 1222

[13] Dubois, L. H.; Zegarski, B. R.; Nuzzo, R. G. *J. Chem. Phys.* **1993**, *98*, 678

[14] Klein, H.; Battaglini, N.; Bellini B.; Dumas, Ph. *Mat. Sci. Eng. C* **2002**, *19*, 279

[15] Ohgi, T.; Sheng, H. Y.; Dong Z. C.; Nejoh, H. *Surf. Sci.* **1999**, *442*, 277

[16] Strong, L.; Whitesides, G. M. *Langmuir* **1988**, *4*, 546

[17] Li, J.; Liang, K. S.; Camillone III, N.; Leung, T. Y. B.; Scoles, G. *J. Chem. Phys.* **1995** *102*,

5012

[18] Camillone III, N.; Chidsey, C. E. D.; Liu, G. Y.; Scoles, G. *J. Chem. Phys.* **1993** *98*, 4234

[19] Poirier, G. E. *Langmuir* **1997** *13*, 2019

[20] Haussling, L.; Michel, B.; Ringsdorf, H.; Rohrer, H. *Agnew. Chem. Int. Ed. Engl.* **1991** *30*, 569

[21] Sun, L.; Crooks, R. M. *J. Electrochem. Soc.* **1991**, *138*, L23

[22] Kim, Y. T.; Bard, A. J. *Langmuir* **1992**, *8*, 1096

[23] Mizutani, W.; Michel, B.; Schierle, R.; Wolf, H.; Rohrer, H. *Appl. Phys. Lett.* **1993**, *63(2)*, 147

[24] Durig, U.; Zuger, O.; Michel, B.; Haussling, L.; Ringsdorf, H. *Phys. Rev. B* **1993** *48*, 1711

[25] Anselmetti, D.; Gerber, Ch.; Michel, B.; Wolf, H.; Gntherodt, H.-J.; Rohrer, H. *Europhys. Lett.* **1993**, *23*, 421

[26] Edinger, K.; Golzhauser, A.; Demota, K.; Woll, C.; Grunze, M. *Langmuir* **1993**, *9*, 4

[27] Fenter, P.; Eberhardt, A.; Eisenberger, P. *Science* **1994**, *266*, 1216

[28] Fenter, P.; Eberhardt, A.; Liang, K. S.; Eisenberger, P. *J. Chem. Phys.* **1996** *106*, 1600

[29] Camillone III, N.; Leung, T. Y. B.; Scoles, G. *Surf. Sci.* **1997**, *373*, 333

[30] Schwartz, P.; Schreiber, F.; Eisenberger, P.; Scoles, G. *Surf. Sci.* **1999**, *423*, 208

[31] Camillone III, N.; Chidsey, C. E. D.; Eisenberger, P.; Fenter, P.; Li, J.; Liang, K. S.; Liu, G. Y.; Scoles, G. *J. Chem. Phys.* **1993**, *99*, 744

[32] Poirier, G. E.; Tarlov, M. J. *Langmuir* **1994**, *10*, 2853

[33] Delamarche, E.; Michel, B.; Gerber, C.; Anselmetti, D.; Guntherodt, H.-J.; Wolf, H.; Ringsdorf, H. *Langmuir* **1994**, *10*, 2869

[34] O'Dwyer, C. et al., unpublished

25

[35] Cullit, B. D. *Elements of X-ray Diffraction*, Addison-Wessely, Reading, 1978

[36] Camillone III, N.; Eisenberger, P.; Leung, B. T. Y.; Schwartz, P.; Scoles, G.; Poirier G. E.; Tarlov, M. J. *J. Chem. Phys.* **1994**, *101*, 11031

[37] Berger, H. *Krist. Tech.* **1976**, *11*, 1171

[38] Raub, E.; Muller, K. *Fundamentals of Metal Deposition*, pp.36-38, Elsevier, Amsterdam, 1967

[39] Uchihashi, T.; Ishida, T.; Komiyama, M.; Ashino, M.; Sugawara, Y.; Mizutani, W.; Yokoyama, K.; Morita, S.; Tokumoto, H.; Ishikawa, M. *Appl. Surf. Sci.* **2000**, *157*, 244

[40] Mar, W.; Klein, M. L. *Langmuir* **1994**, *10*, 188

[41] Bareman, J. P.; Klein, M. L. *J. Phys. Chem.* **1990**, *94*, 5202

[42] Ryckaert, J. P; McDonald, I. R.; Klein, M. L. *Mol. Phys.* **1989**, *67*, 957

[43] Touzov, I.; Gorman, C. B. *J. Phys. Chem. B* **1997**, *101*, 5263

Figure captions

Fig.1

Schematic representation of the alkanethiol assembly on Au{111}. (a) Schematic illustration of molecules arranged in the $(\sqrt{3} \times \sqrt{3})$R30^0 hexagonal packing arrangement. White circles are Au atoms. (b) Schematic illustration of alkanethiol molecules (shaded circles) on Au{111} (white circles) in a $(3 \times 2\sqrt{3})$ lattice. The gray circles represent the methyl head rotated $\pm50^0$ about its main axis. (c) Schematic illustration of alkanethiol molecules in a (4×2) superlattice. The gray circles represent the methyl head rotated $\pm50^0$ about its main axis. the arrows represent the direction of the cross-sectional schematics.

Fig.2

The GIXRD spectrum of the Au layer. The spectrum was acquired at grazing incidence to determine the preferential orientation of the grains without substrate contributions. On a logarithmic scale, no discernable peaks from {200}, {220} or {311} reflections of the Au lattice could be observed. *inset* Physical rocking curve of the Au layer for the {111} peak.

Fig.3

(a) 2 μm $\times$ 2 μm tapping mode survey AFM image of the sputtered Au surface immediately prior to immersion in the alkanethiol bath solution. (b) 0.16 μm $\times$ 0.16 μm higher magnification image of (a) showing multiple grain boundaries.

Fig.4

385 nm $\times$ 385 nm tapping mode AFM image of the Au{111} surface shown in height-

mapped grayscale, featuring 0.25 nm high monoatomic terraces and grain boundaries. The terrace edges are delineated by the {111} planes of the Au lattice. Examples of monoatomic depressions in the Au surface are highlighted by arrows.

Fig.5

60 nm × 60 nm molecular resolution STM image of the 1-nonanethiol SAM on the sputtered Au{111} surface showing the mosaic-like domain network. The dark spots indicated by arrows are single-atom-deep depressions in the Au surface and the dark fissures (indicated by arrowheads) are examples of alkanethiol domain walls. Domains of two symmetry-equivalent orientations are indicated by dashed lines aligned with the unit cell short-axis.

Fig.6

(a) 32.5 nm × 32.5 nm molecular resolution STM image of the 1-nonanethiol monolayer showing a SAM domain boundary between two domains on a single Au grain. Domains of two symmetry-equivalent orientations are indicated by arrows aligned with the unit cell short-axis. (b) 32.5 nm × 32.5 nm STM image where a SAM domain boundary can be observed. This boundary exists between two neighboring Au grains. The dark spots (shown by dashed arrows) are monoatomic depressions in the Au surface. The domains boundaries are highlighted by arrowheads.

Fig.7

High resolution STM and AFM images of the molecular packing arrangement of the SAM on Au(111). (a) STM image of the molecular overlayer in constant height mode with

a sample bias of 1.5 V. The characteristic zig-zag pattern of the (4×2) superlattice is highlighted by open circles. (b) Non-contact AFM image with molecular resolution of the same surface, showing the change in packing arrangement from (4×2) to the $(3 \times 2\sqrt{3})$ a $(\sqrt{3} \times \sqrt{3})R30^0$ hexagonal lattice with increased tip distance from the surface. The nearest-neighbor molecules are commensurate with the Au{111} lattice along the [112] directions.

Fig.8

(a) Schematic representations of the three classes of conformations that 1-nonanethiol molecular chains can take. C represents a carbon atom and H represents a hydrogen atom. (b) Representation of a alkanethiol molecule in an all-trans configuration. The orientation of the molecule is defined by the molecular tilt $\theta = 30^0$, the angle of rotation of the C-C-C planes about the molecular axis $\theta = 50^0$ and the angle of precession about the surface normal $\chi = 12^0$ away from the nearest neighbor position.

Fig.9

Non-contact AFM images of the 1-nonanethiol monolayer on Au{111}. (a) The nearest neighbor (along the [112] directions of the Au lattice) and (b) next-nearest neighbor molecules (along the [111] directions of the Au lattice) are highlighted and the corresponding cross-sectional line scan profiles are shown. The repeat distances, as a function of the interatomic Au-Au lattice constant, $a = 0.29$ nm, are also highlighted in the line scan profiles.

Fig.10

(a) Molecular resolution STM image showing detail of a translational boundary in a

1-nonanethiol lattice. The data is presented with individual height-mapped grayscale for each terrace level for clarity of contrast. The translation of a (4×2) superlattice is highlighted. (b) STM image showing multiple monoatomic Au{111} terrace edges. These edges are delineated by the {111} planes of the Au lattice and are aligned in the [111] directions. (c) STM evidence of a rotational boundary in the monolayer. The dashed line highlights the boundary and is parallel to the Au[112] direction. The rotated $(3 \times 2\sqrt{3})$ unit mesh is also highlighted. The arrow indicates the presence of a prominent Au step.

Fig.11

40 nm $\times$ 40 nm STM image of the 1-nonanethiol on Au{111}, where a large number of non-uniformities such as domain boundaries, pinholes and monoatomic depressions are observed.

Fig.12

30 nm $\times$ 30 nm molecular resolution non-contact AFM image of the boundary between two SAM domains. The domain boundary is indicated by the arrow. The image was acquired in tapping mode with a tip with low spring constant (0.12 nN nm^{-1}).

(√3 × √3)R30⁰

(√3 × √3)R30⁰

(3 × 2√3)

(3 × 2√3)

(4 × 2)

(4 × 2)

Fig. 1

Fig. 2

32

(a)

400nm

(b)

55nm

Fig. 3

33

100 nm

Fig. 4

10 nm

Fig. 5

Fig. 6

Fig. 7

(a) trans / cis (eclipsed) / gauche

(b)

Fig. 8

Fig. 9

(a)

(4 × 2)

(b)

5 nm

(c)

Au step

[111]

[112]

Fig. 10

5 nm

Fig. 11

5 nm

Fig. 12

TOC Image